(12) INTERNATIONAL APPLICATION PUBLISHED UNDER THE PATENT COOPERATION TREATY (PCT)

(19) World Intellectual Property Organization
International Bureau

(43) International Publication Date
22 June 2017 (22.06.2017)

WIPO | PCT

(10) International Publication Number
WO 2017/103783 A1

(51) International Patent Classification:
H01M 4/38 (2006.01) *H01M 4/62* (2006.01)
H01M 4/485 (2010.01)

(21) International Application Number:
PCT/IB2016/057574

(22) International Filing Date:
13 December 2016 (13.12.2016)

(25) Filing Language: English

(26) Publication Language: English

(30) Priority Data:
62/266,757 14 December 2015 (14.12.2015) US

(71) Applicant: **KING ABDULLAH UNIVERSITY OF SCIENCE AND TECHNOLOGY** [SA/SA]; 4700 King Abdullah University of Science and Technology, Thuwal, 23955-6900 (SA).

(72) Inventors: **LI, Lain-Jong**; 4700 King Abdullah University of Science and Technology, Thuwal, 23955-6900 (SA). **MING, Jun**; 4700 King Abdullah University of Science and Technology, Thuwal, 23955-6900 (SA).

(81) Designated States *(unless otherwise indicated, for every kind of national protection available)*: AE, AG, AL, AM, AO, AT, AU, AZ, BA, BB, BG, BH, BN, BR, BW, BY, BZ, CA, CH, CL, CN, CO, CR, CU, CZ, DE, DJ, DK, DM, DO, DZ, EC, EE, EG, ES, FI, GB, GD, GE, GH, GM, GT, HN, HR, HU, ID, IL, IN, IR, IS, JP, KE, KG, KH, KN, KP, KR, KW, KZ, LA, LC, LK, LR, LS, LU, LY, MA, MD, ME, MG, MK, MN, MW, MX, MY, MZ, NA, NG, NI, NO, NZ, OM, PA, PE, PG, PH, PL, PT, QA, RO, RS, RU, RW, SA, SC, SD, SE, SG, SK, SL, SM, ST, SV, SY, TH, TJ, TM, TN, TR, TT, TZ, UA, UG, US, UZ, VC, VN, ZA, ZM, ZW.

(84) Designated States *(unless otherwise indicated, for every kind of regional protection available)*: ARIPO (BW, GH, GM, KE, LR, LS, MW, MZ, NA, RW, SD, SL, ST, SZ, TZ, UG, ZM, ZW), Eurasian (AM, AZ, BY, KG, KZ, RU, TJ, TM), European (AL, AT, BE, BG, CH, CY, CZ, DE, DK, EE, ES, FI, FR, GB, GR, HR, HU, IE, IS, IT, LT, LU, LV, MC, MK, MT, NL, NO, PL, PT, RO, RS, SE, SI, SK, SM, TR), OAPI (BF, BJ, CF, CG, CI, CM, GA, GN, GQ, GW, KM, ML, MR, NE, SN, TD, TG).

Declarations under Rule 4.17:

— *as to applicant's entitlement to apply for and be granted a patent (Rule 4.17(ii))*

Published:

— *with international search report (Art. 21(3))*

WO 2017/103783 A1

(54) Title: LITHIUM-SULFUR BATTERY, A DUAL BLOCKING LAYER, METHODS OF MAKING, AND METHODS OF USE THEREOF

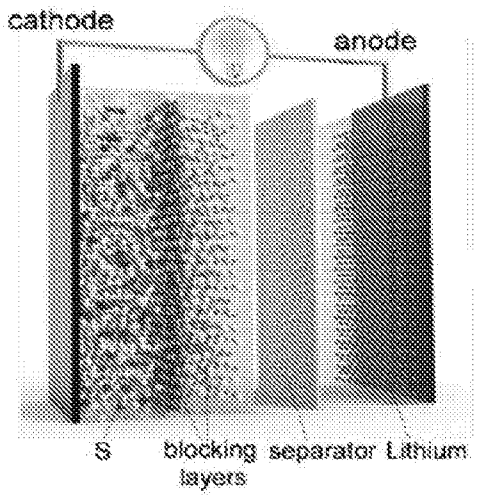

Fig. 1A

(57) Abstract: The present disclosure provides for a lithium-sulfur battery with a dual blocking layer between the anode and cathode, providing for high storage capacity and improved performance.

LITHIUM-SULFUR BATTERY, A DUAL BLOCKING LAYER, METHODS OF MAKING, AND METHODS OF USE THEREOF

CROSS-REFERENCE TO RELATED APPLICATIONS

This application claims the benefit of and priority to U.S. Provisional Application Serial No. 62/266,757, having the title "LITHIUM-SULFUR BATTERY, A DUAL BLOCKING LAYER, METHODS OF MAKING, AND METHODS OF USE THEREOF," filed on December 14, 2015, the disclosure of which is incorporated herein in by reference in its entirety.

BACKGROUND

Sulphur (S) has been recognized as a promising electrode material for next generation Li-S batteries owing to its high theoretical specific capacity. However, the problem of low sulphur utilization and severe capacity fading still remain to be addressed before their commercialization.

SUMMARY

The present disclosure provides for a lithium-sulfur battery with a dual blocking layer between the anode and cathode, providing for high storage capacity and improved performance.

An embodiments of the present disclosure provides for a battery, among others, that includes: an anode and a cathode, wherein a dual blocking layer is disposed on the cathode. The dual blocking layer is a graphite/$Li_4Ti_5O_{12}$, and the dual layer is between the anode and the cathode.

An embodiment of the present disclosure includes a battery, among others, that includes: an anode and a cathode, wherein a dual blocking layer is disposed on the cathode. The dual blocking layer is a conductive material and lithium storage medium, and the dual layer is between the anode and the cathode.

Other compositions, apparatus, methods, features, and advantages will be or become apparent to one with skill in the art upon examination of the following drawings and detailed description. It is intended that all such additional compositions, apparatus, methods, features and advantages be included within this description, be within the scope of the present disclosure, and be protected by the accompanying claims.

BRIEF DESCRIPTION OF THE DRAWINGS

Further aspects of the present disclosure will be more readily appreciated upon review of the detailed description of its various embodiments, described below, when taken in conjunction with the accompanying drawings.

Figures 1A-D show the scheme of hybrid lithium-sulphur battery and electrochemical performances. Fig. 1A is a schematic for the hybrid lithium-sulphur battery, in which the sulphur-rich cathode of 90 wt% sulphur-10 wt% Super P® (conductive carbon black, TIMCAL) composite was covered by the layer of graphite and LTO. Voltage vs. capacity profiles of the sulphur rich electrode covered by the layer of graphite and LTO. Fig. 1B shows graphite/LTO and Fig. 1C shows LTO/graphite under different rate. Fig. 1D shows rate capability and cycle performance of hybrid battery using the graphite/LTO blocking layer. The inset of Fig. 1D is the typical voltage vs. capacity profiles at the rate of 1 C.

Figures 2A-G demonstrate surface morphology of sulphur rich cathode covered by the layer of graphite and LTO. Figs. 2A, 2B, and 2E and is a digital photograph, scanning electron microscope (SEM) and energy-dispersive X-ray mapping of the pristine sulphur rich cathode, and that can be covered respectively by (Fig. 2C, 2F) graphite and (Fig. 2D, 2G) graphite/LTO layer. Scale bar: 100 μm. The color of blue, yellow, red (Fig. 2F), green and pink-white (Fig. 2G) (and corresponding shades of grey) present elements of aluminium, sulphur, carbon, fluorine and steric situation of LTO respectively.

Figures 3A-D are electrochemical analyses. Fig. 3A plots open-circuit voltage *vs.* time curve, Fig. 3B illustrates cyclic voltammetry, Fig. 3C illustrates the plot of normalized peak current (i_p) with the square root of the scan rate ($\upsilon^{1/2}$) and Fig. 3D illustrates the Niquist plot of battery using a graphite/LTO, a LTO/graphite layer and pristine electrode without a blocking layer.

Figures 4A-I illustrate visual observation and operando Raman analysis. Fig. 4A shows photos for the cycled batteries with a graphite/LTO layer, Fig. 4B shows a LTO/graphite layer and Fig. 4C shows pristine electrode after the 1st, 3rd, 7th, 25th and 50th charge/discharge cycles. Fig. 4D is a photo of the home-made glass tube battery. Fig. 4E shows a typical operando Raman spectra of the electrolyte after cycling in the battery using graphite/LTO as blocking layer. Fig. 4F shows relative intensity of background at 2500 cm^{-1} calculated based on the equation of $\Delta I_{2500\ cm\text{-}1}/I_{\upsilon C\text{-}H\ (2883\ cm\text{-}1)}$, in which in which $\Delta I_{2500\ cm\text{-}1}$ is the difference of Raman intensities of baseline at 2500 cm^{-1} comparing to the 1st cycle while $I_{\upsilon C\text{-}H(2883\ cm\text{-}1)}$ is the C-H vibration at 2883 cm^{-1}. Raman spectrum (500-700 cm^{-1}) of the electrolyte in the batteries using blocking layers of (Fig. 4G) graphite/LTO, (Fig. 4H) LTO/graphite and (Fig. 4I) pristine electrode at the 1st, 3rd, 7th, 25th, 35th, 50th cycles.

Figures 5A-H show morphology of the cycled electrode and proposed reaction process. Scanning electron microscope (SEM) and energy-dispersive X-ray mapping of (Fig. 5A) a pristine electrode cycled for (Fig. 5B) 25^{th}, (Fig. 5C) 50^{th} cycles (inset is the photo of cycled electrode) and (Fig. 5D) the schematic illustration for electrode change after cycling. The charge flow in the figure represent the discharge process. (Fig. 5E) Sulphur-rich cathode covered by the graphite/LTO layer cycled for (Fig. 5F) 25^{th}, (Fig. 5G) 50^{th} cycles (inset is the photo of electrode) and (Fig. 5H) the proposed reaction process. Black and red arrow represent the diffusion of lithium ions and transport of electronics. Scale bar length is 50 μm.

Figures 6A-E illustrate electrochemical performances of batteries without and with different blocking layer. Fig. 6A shows cycling performances of battery without and with different blocking layer. Typical voltage *vs.* capacity profiles of batteries (Fig. 6B) without blocking layer and with (Fig. 6C) graphite, (Fig. 6D) LTO and (Fig. 6E) graphite/LTO layers at the high rate of 1C. The voltage polarization of batteries using blocking layer and without any blocking layer were compared at the capacity of 500 mAh g^{-1} and 0.3 mAh g^{-1} respectively.

Figures 7A-C demonstrate electrochemical performances of battery at high temperature of 60 ^{o}C. (Fig. 7A) Comparative cycle ability and typical voltage *vs.* capacity profiles of batteries with using blocking layers of (Fig. 7B) graphite/LTO and (Fig. 7C) LTO/graphite under the rate of 1C at the high temperatures of 60 ^{o}C.

Figure 8 is an embodiment of a battery, with parts labeled (a) Hollow glass tube, (b) long steel with polytetrafluoroethylene (PTFE) neck, between which the anode of lithium, cathode of sulfur and separator were placed to assemble the battery, (c) red cap which were used to seal the PTFE neck, (d) spare hollow tubes which are available to fill and exhaust gas if necessary, such as in the study of the lithium-oxygen battery. In this hybrid lithium battery, the small hollow tubes of (d) were sealed. The position of (e) on the hollow glass tube is a projection with the flat surface for holding and investigating the electrolyte by laser during the collection of Raman spectrum. Right inset is a photo of cycled battery in the test.

Figures 9A-B provide Operando Raman spectrum of electrolyte as cycling. Batteries with using (Fig. 9A) graphite/LTO and without blocking layer (Fig. 9B) tested under the scan rate of 0.1 mV s^{-1}.

DETAILED DESCRIPTION

Before the present disclosure is described in greater detail, it is to be understood that this disclosure is not limited to particular embodiments described, as such may, of course, vary. It is also to be understood that the terminology used herein is for the purpose of

describing particular embodiments only, and is not intended to be limiting, since the scope of the present disclosure will be limited only by the appended claims.

Where a range of values is provided, it is understood that each intervening value, to the tenth of the unit of the lower limit (unless the context clearly dictates otherwise), between the upper and lower limit of that range, and any other stated or intervening value in that stated range, is encompassed within the disclosure. The upper and lower limits of these smaller ranges may independently be included in the smaller ranges and are also encompassed within the disclosure, subject to any specifically excluded limit in the stated range. Where the stated range includes one or both of the limits, ranges excluding either or both of those included limits are also included in the disclosure.

Unless defined otherwise, all technical and scientific terms used herein have the same meaning as commonly understood by one of ordinary skill in the art to which this disclosure belongs. Although any methods and materials similar or equivalent to those described herein can also be used in the practice or testing of the present disclosure, the preferred methods and materials are now described.

As will be apparent to those of skill in the art upon reading this disclosure, each of the individual embodiments described and illustrated herein has discrete components and features which may be readily separated from or combined with the features of any of the other several embodiments without departing from the scope or spirit of the present disclosure. Any recited method can be carried out in the order of events recited or in any other order that is logically possible.

Embodiments of the present disclosure will employ, unless otherwise indicated, techniques of chemistry, inorganic chemistry, material science, and the like, which are within the skill of the art. Such techniques are explained fully in the literature.

The following examples are put forth so as to provide those of ordinary skill in the art with a complete disclosure and description of how to perform the methods and use the compositions and compounds disclosed and claimed herein. Efforts have been made to ensure accuracy with respect to numbers (*e.g.*, amounts, temperature, etc.), but some errors and deviations should be accounted for. Unless indicated otherwise, parts are parts by weight, temperature is in °C, and pressure is in atmosphere. Standard temperature and pressure are defined as 25 °C and 1 atmosphere.

Before the embodiments of the present disclosure are described in detail, it is to be understood that, unless otherwise indicated, the present disclosure is not limited to particular materials, reagents, reaction materials, manufacturing processes, or the like, as such can vary. It is also to be understood that the terminology used herein is for purposes of describing particular embodiments only, and is not intended to be limiting. It is also possible

in the present disclosure that steps can be executed in different sequence where this is logically possible.

It must be noted that, as used in the specification and the appended claims, the singular forms "a," "an," and "the" include plural referents unless the context clearly dictates otherwise. Thus, for example, reference to "a support" includes a plurality of supports. In this specification and in the claims that follow, reference will be made to a number of terms that shall be defined to have the following meanings unless a contrary intention is apparent.

Discussion

Embodiments of the present disclosure provide for batteries including dual blocking layers, lithium-sulfur batteries, methods of making dual blocking layers, methods of making lithium-sulfur batteries, and the like. Embodiments of the present disclosure can be advantageous since the use of the dual blocking layer can efficiently stabilize the cathode (*e.g.*, sulfur cathode) with higher utilization (*e.g.*, sulfur utilization) and enhance the capacity of battery contributed by the unique blocking layer (*e.g.*, graphite/LTO). Because of the additional capacity and work voltage plateau contributed from the blocking layer, embodiments of the present disclosure provide for a battery (*e.g.*, an advanced lithium-sulfur battery) with higher capacity, improved stability and more voltage plateaus are introduced.

Furthermore, the dual blocking layer can work with a variety of electrode materials with diverse voltage plateaus. In an exemplary embodiment, the dual blocking layer can be used to stabilize lithium-sulfur batteries and particularly enrich lithium batteries, which is significant for providing more choice in energy devices. Embodiments of the present disclosure provide lithium-sulfur batteries with superior stability, enhanced capacity and more voltage plateau, which can be used for portable electronic devices, grid storage and electric vehicles (EV).

Lithium-sulfur batteries are considered as the next generation high performance battery. However, the low sulfur utilization and sever capacity fading are parameters that need to be addressed. Embodiments of the present disclosure provide for dual blocking layers that can enhance overall performance of the batteries, in particular lithium batteries, hybrid lithium batteries (*e.g.*, lithium-sulfur batteries).

An embodiment of the present disclosure includes a dual blocking layer having a conductive material and a lithium storage medium, where conductive material and the lithium storage medium are immediately adjacent one another. The dual layer is between the anode and the cathode. In an embodiment, the lithium storage medium can be a medium having a storage capacity of about 1.0-2.0V.

In an embodiment the conductive material can be a carbon based material, a conductive polymer, or a combination thereof. In an embodiment, the carbon based material

can be: graphite, Super P® (conductive carbon black, TIMCAL), active carbon, activated carbon, acetylene black, carbon nanotubes, graphene, graphene oxide, or a combination thereof. In an embodiment, the conductive polymer can be: polyaniline, polypyrrole, polythiophenes, PEDOT:PSS, chitosan, or a combination thereof.

In an embodiment, the lithium storage medium can be: $LI_4Ti_5O_{12}$, TiO_2, MoO_2, Fe_2O_3, Co_3O_4, MoS_2, or a combination thereof. In a particular embodiment, the dual blocking layer can be graphite/$Li_4Ti_5O_{12}$ (abbreviated as LTO) or spinel $Li_4Ti_5O_{12}$. In an embodiment, the dual blocking layer is included in a battery such as a lithium battery or a hybrid lithium battery (*e.g.*, lithium-sulfur battery). The dual blocking layer can be disposed on the cathode so that it is between the cathode and the anode. In a particular embodiment, the dual blocking layer can be disposed on the cathode so that the conductive material (*e.g.*, graphite) is adjacent the cathode (*e.g.*, sulfur cathode). In an embodiment, the dual blocking layer can have a thin thickness (*e.g.*, several μm, about 1 to 5 or about 1 to 3 μm) or a thick thickness (*e.g.*, over/less 100 μm, or about 75 to 125 μm) depending upon the specific requirement of the device. The other dimensions (*e.g.*, length, width) can vary depending upon the dimensions of the battery.

As mentioned above, an embodiment of the present disclosure includes a lithium-sulfur battery that includes the dual blocking layer (*e.g.*, graphite/LTO). In an embodiment the sulfur cathode and the lithium cathode can include those known in the art. In an embodiment, the battery can include an anode (*e.g.*, lithium metal), an electrolyte (*e.g.*, an organic solvent containing lithium salt), and a cathode of the present disclosure, where the electrolyte is disposed between the anode and cathode and the dual blocking layer is adjacent the cathode so that it is between the lithium electrolyte and the anode. In a particular embodiment, the battery includes a structure such as anode-separator-dual blocking layer/cathode in electrolyte such as shown in the Example. In an embodiment the electrolyte can be a solid electrolyte or a liquid electrolyte. If a solid electrolyte is used, the position of solid electrolyte will replace of the position of separator, in which the solid electrolyte can also behaviors as separator for cathode and anode.

In an embodiment, the lithium-sulfur battery has a capacity about 1800 to 2000 mAh g^{-1} or more. In an embodiment, the lithium-sulfur battery provides multi-voltage platforms from 2.35 V, 2.1 V to 1.55 V. In an embodiment, the lithium-sulfur battery can have an energy density of about 3800 to 4000 Wh kg^{-1} or more, which is about ten times higher or more than a lithium ion battery and also superior than the theoretical 2600 Wh kg^{-1} of lithium-sulphur battery. In an embodiment, the dual blocking layer can obtain about 90 to 100 % utilization or about 100% utilization of the sulfur cathode. In addition, the lithium-sulfur battery including the dual blocking layer can have a capacity of about 1200 to 1250 mAh g^{-1}

at the high rate of about 1° C with endurable cycle life over about 100 cycles. Additional details are provided in Example 1.

In an embodiment, the dual blocking layer can be prepared by a two-step coating process. First, a slurry of sulfur and conducting carbon with high sulfur content (i.e., about 80 wt%-100 wt% sulfur) was cast on the current collector of aluminum foil. After drying the electrode, a slurry composed of graphite/polyvinylidene difluoride (PVDF) (9/1, w/w) and LTO/Super P/PVDF (8/1/1, w/w/w) in N-Methyl-2-pyrrolidone (NMP) were cast on top of sulfur electrode step-by-step respectively. The sulfur electrode with dual blocking layer is formed after a complete dry.

Example 1

Herein, we present a dual blocking layer of graphite/$Li_4Ti_5O_{12}$ (LTO) to stabilize the sulphur-rich cathode (90 wt% sulphur) with 100% utilization of sulphur is obtained. The graphite/LTO layer not only suppresses the dissolution/migration of polysulfide efficiently but also contributes additional capacity. As a result, an advanced hybrid lithium sulfur battery with an exceptional capacity of 1866 mAh g_s^{-1} at 0.1C and successive voltage platforms from 2.35 V, 2.1 V to 1.55 V is introduced, giving rise to impressive energy density of 3863 Wh kg^{-1}. The extremely high rate capacity of 1226 mAh g_s^{-1} with stable cycle ability over 100 cycles at 1C are also obtained even at high temperature. The color change of electrolyte as cycling is further characterized by the operando Raman analysis, and a reaction mechanism of the sulphur-rich cathode is presented. This new hybrid lithium battery with dual layer concept can extend to marry different voltage plateau of electrode in one cell and can open a way for providing higher capacity and more voltage platforms available in energy storage and conversion devices.

The development of high capacity rechargeable battery has been pursued intensively in the past two decades, particularly with the strong demand from portable electronic devices and electric vehicles.[1,2] Although recent lithium-air battery may potentially provide an infinite capacity (without considering the weight of oxygen for the reaction of $O_2 + 2Li^+ + 2e^- \rightarrow Li_2O_2$), the typical capacity usage is strictly controlled (*e.g.*, < 2000 mAh $g_{cathode}^{-1}$) to avoid the accumulation of lithium peroxides on cathodes (*e.g.*, carbon,[3] metal oxide[4,5]) since the excess lithium peroxides may lead to the expiry of battery. More efforts are required before it can serve for practical applications.[6] Alternatively, lithium-sulphur battery with the high theoretical capacity of 1675 mAh g^{-1} (i.e., $1/8S_8 + 2Li^+ + 2e^- \rightarrow Li_2S$) has been considered promising to replace the commonly used metal oxide lithium-ion batteries.[7-12] However, during the discharge process the solid sulphur (S_8) always forms soluble lithium polysulfide (Li_2S_x, x = 4-8) intermediates which will diffuse into the electrolyte and may deposit on anodes to proceed further reactions (i.e., $Li_2S_4 \rightarrow 2Li_2S_2 \rightarrow 4Li_2S$).[13-15] The formation of

insoluble/insulating Li_2S on anodes, particularly those directly react with lithium anode in self-discharge,[13] is the main cause of sulphur loss and internal resistance increase, thereby leading to the low sulphur utilization and severe capacity fading.

To reduce the loss of active sulphur materials in cathode, encapsulation of sulphur in porous and/or hollow structures of different forms such as carbon (e.g., mesoporous carbon,[16,17] hollow carbon,[18,19] carbon nanotubes,[20,21] graphene (oxide)[22]), metal oxide[23] and polymers[24,25] has been reported. These approaches have shown success in suppressing the dissolution and diffusion of polysulphides in electrolytes and the deposition of Li_2S on anodes. Other versatile strategies have also been developed to attack the sulphur dissolution issues, including (1) choosing a stronger binder,[26] (2) seeking polymeric[27,28] and solid separator[29], (3) adding additives[30,31] and/or compensation of polysulphide,[32,33] (4) using porous current collector[34] and/or inserting an interlayer in the cell configuration[35,36] and (5) depositing a protective layer (e.g., carbon,[37] or polymer[38]) on the separator or on the anode.[39] These approaches have substantially retained the polysulphides in cathodes and thus improved the cycle life of Li-S cells. While the materials applied in these strategies play the role of either blocking the diffusion of polysulphides or reducing the internal resistance of batteries, but they do not contribute to the capacity at all. Therefore, it is substantially attractive to explore the possibility to use a lithium storage medium as the sulphur blocking layer as well as a battery capacity booster.

Herein we note that a spinel lithium titanate $Li_4Ti_5O_{12}$ (abbreviated as LTO) layer not only efficiently retards the sulphur dissolution but also allows fast lithium ion diffusion. Further, LTO is a "zero-strain" lithium ion host;[40] thus, it can provide additional capacity with a continued discharge voltage at 1.55 V to the lithium-sulphur battery. In this report, we explore a unique dual blocking layer, LTO on graphite, which enables nearly 100% sulphur utilization for a sulphur rich cathode (i.e., 90 wt% sulphur with 10 wt% Super P simply prepared by physical mixing). This new type of blocking layer gives rise to an endurable hybrid Li-S battery with multi-voltage platforms (i.e., 2.35 V, 2.1 V and 1.55 V) and an extremely high capacity of 1866 mAh g^{-1} (nearly the sum of the full capacities of S and LTO). Such an approach significantly boosts up the overall capacity, improves the cycle stability and demonstrates the possibility of using hybrid structure/material to largely enhance the performance of battery. Further, the change of electrolytes and electrodes with cycling were characterized by the operando Raman analysis and *ex-situ* scanning electron microscope (SEM), where the S-dissolution from the sulphur rich cathode was carefully studied.

Experimental

Preparation of electrode

Commercial sulphur (Sigma Aldrich, purity higher than 99.5%) and Super P with the mass ratio of 9:1 were mixed and melted at 250 °C in sealed glass bottle, giving rise to a grey bulk solid which was then crushed by motor and re-melted again. This procedure was repeated for three times before the collection of 90wt% S-10wt% Super P composite. As-prepared composite and polyvinylidene difluoride (PVDF) were mixed in the N-Methyl-2-pyrrolidone (NMP) to form a slurry and then casted on the Aluminium foil. Drying the electrode at 40 °C in vacuum oven, then graphite and LTO were coated on the sulphur electrode in a layer-by-layer manner. The graphite was purchased from the company of Fisher Scientific and the $Li_4Ti_5O_{12}$ was synthesized accordingly.[41] The graphite and $Li_4Ti_5O_{12}$ layers were the mixture of graphite/PVDF (w/w, 9/1) and LTO/Super P/PVDF (w/w/w, 8/1/1) respectively, which were suspended in the NMP first and then casted by the same procedures as that of sulphur electrode. Average area mass density of sulphur, graphite and LTO are controlled at around 1.5, 0.75 and 2.64 mg cm^{-2}. The electrodes were punched into Ø13 mm circular discs after a complete dry and then assemble the battery. The tuneable mass density of LTO here is about 2.64 mg cm^{-2} (i.e., only 3.50 mg for Ø13 mm electrode), which is much lighter than most intercalated carbon blocking layer.[35]

Electrochemical test

The performance of the batteries was characterized by the 2032-type coin cell, and they were assembled in the Ar filled glovebox in which the content of oxygen and moisture was strictly controlled below 0.5 ppm. The lithium sulphur battery has the configuration of electrode | separator | lithium-metal model using the electrolyte of 1.0 M bis(trifluoromethane)sulfonamide lithium salt (LiTFSI) in the mixture of 1,3-dioxolane (DIOX)/1,2-dimethoxyethane (DME) (V/V, 1:1) (1wt.% $LiNO_3$ *vs.* LiTFSI). The amount of electrolyte for each cell is controlled at 150 µL. Galvanostatic cycling was conducted in the voltage window of 1.5-3.2 V using the Arbin battery testing system USA. The specific capacity of electrode was calculated based on the mass of sulphur. Cyclic voltammetry (CV) was carried out under the scan rate of 0.075-0.25 mV s^{-1} and electrochemical impedance spectroscopy (EIS) was acquired over a frequency range of 200 kHz–10 mHz using the instrument of Multi-Channel Potentiostat BioLogic VMP3.

Characterizations

The surface morphology of electrode was characterized by the field emission scanning electron microscope (FESEM, FEI Quanta 200), operated at 5 kV and 2.5 mA. The elemental distribution of sulphur, carbon, binder of PVDF and $Li_4Ti_5O_{12}$ were analysed by the energy-dispersive X-ray (EDX) mapping, operated at 10 kV and 6 mA. The operando Raman spectrum of electrolyte was carried out by a specific glass tube battery as we designed and the spectrum was collected on Witec alpha 300R Raman spectrometer at a 514 nm excitation wavelength. The cyclic voltammetry of glass tube battery was performed within the voltage of 1.5-3.2 V under the scan rate of 0.1 mV s^{-1}.

Results and Discussion

Hybrid Lithium-Sulphur Battery

Figures 1A-D present the hybrid lithium-sulphur battery composed of a Li metal as the anode and sulphur as the cathode, where a composite blocking layer (a graphite layer followed by the deposition of a LTO layer, abbreviated as graphite/LTO) is applied to retard the S-dissolution. At the rate of 0.1 C, the sulphur utilization can achieve nearly 100% with the capacity of 1675 mAh g_s^{-1} (based on the weight of sulphur). The perfect discharge-charge curve has very flat and smooth voltage platforms at around 2.35V and 2.1V and an extremely low polarization of 146.7 mV which is much lower than most published results.[8-10] In addition to the full capacity from sulphur, the LTO layer also contributes the additional capacity around 191 mAh g^{-1} at 1.55 V, which largely enhances the battery capacity to 1866 mAh g^{-1} and achieves an extremely high energy density of 3863 Wh kg^{-1} (Figure 1B). In theory, the reactions from solid sulphur to soluble Li_2S_4 can give rise to a total capacity of 419 mAh g^{-1}, and then a sum capacity of 1256 mAh g^{-1} was delivered in the further reactions (i.e., $Li_2S_4 \rightarrow Li_2S_3/Li_2S_2 \rightarrow Li_2S$) (Table 1). But, there are very few reports succeeding in getting a theoretical capacity because of the serious self-discharge (e.g., chemical reactions between dissolved polysulphides (Li_2S_x, x = 2-8) and lithium metal).[42-44] To analysis the result, we divide the discharge curves into three regions including the 1st plateau around 2.35 V (i.e., Q_1), a slope area from 2.35 V to 2.1 V (i.e., Q_{slope}), and the rest of the discharge area from 2.1 V to 1.56 V (i.e., Q_2),[45] and the capacities are 321, 218 and 1136 mAh g^{-1} respectively (Figure 1B). Clearly, the value of Q_{slope} for our current study is among the highest compared with existing reports (Table 2), demonstrating that the dissolved Li_2S_x (x = 3-8) are well trapped in the covered layer and then it can give rise to more capacity at a relatively high voltage. Another important parameter of $(Q_1 + Q_{slop})/Q_2$ is also presented.[35,45]

Generally, the higher value it is, the better ability of cathode to hold the sulphur species should be. In this report, the value of 0.474 is relatively higher than most reported S-cathode, confirming the superior protection ability of graphite/LTO dual layer. With the increasing charge/discharge rate, the high capacities of 1411, 1256, 1076 and 716 mAh g^{-1} at the rate of 0.25, 0.5, 1, 2.5 C are obtained, and particularly the battery has no obvious voltage-decay even to the high rate of 2.5 C.[46,47] Meanwhile, the capacity around 1.55V increases to around 280 mAh g^{-1} with the progress of cycling, which may result from a full activation of LTO and the reduction of accumulated Li_2S_2 to Li_2S trapped in the dual blocking layer.

Note that the sequence of the dual blocking layer critically determines the performance of lithium-sulphur batteries. If the LTO is first deposited on the sulphur cathodes and followed by the graphite (abbreviated as LTO/graphite), the sulphur utilization of battery is reduced to 87.7% at 0.1 C with a larger polarization of 486.3 mV (*vs.* 398.1 mV of graphite/LTO) at 2.5 C (Figure 1C). Also, the battery shows lower capacities of 1385, 1194, 869 and 632 mAh g^{-1} at 0.1, 0.25, 0.5, 1 and 2.5C respectively. Particularly, the LTO/graphite layer almost has no capacity contribution at the high rate such as at 1C, under which the graphite/LTO layer still exhibits a high capacity contribution of 226 mAh g^{-1}. The higher sulphur utilization of battery with graphite/LTO layer may benefit from the faster transport of charges endowed by the embedded graphite layer, and the higher LTO capacity contribution of graphite/LTO can be ascribed to the direct contact LTO to the electrolytes, where the dissociated lithium ion can be inserted to the LTO with less steric hindrance compared with the case of LTO/graphite. The need for dual graphite/LTO layer is further demonstrated by the comparative studies of the cathodes using single and without any blocking layer. For example, the battery using the graphite/LTO blocking layer demonstrates the highest capacity of 1226 mAh g^{-1} and the lowest polarization of 289.4 mV at 1 C, which are much better than those using only graphite (i.e., 905 mAh g^{-1}, 335.6 mV), only LTO (i.e., 1050 mAh g^{-1}, 384.3 mV) and the pristine electrode without any blocking layer (i.e., 0.7 mAh g^{-1}, 1577.1 mV) (Figure Fig. 6A-E). Even suffering from the harsh rate test, the cathode with graphite/LTO layer can recover and further cycle at 1 C over 100 cycles with a high capacity of 1005 mAh g^{-1} and a good capacity retention of 82% (Figure 1D). The versatile discharge-charge curves with three flat voltage platforms around 2.35 V, 2.1 V and 1.55 V would be attractive for enriching the kind of rechargeable batteries (inset of Figure 1D), and this new concept of combining voltage plateaus from different materials will open a way for energy storage and conversion devices. Besides, the cell with the graphite/LTO blocking layer is sustainable even when it is cycled at 60 °C, where the initial cycle capacity

can reach 1551 mAh g^{-1} (Figures 7A-C), three times higher than graphene-based electrode.[48]

It is noted that introducing a blocking layer with available lithium ion storage capacity is a new approach and the process is simple, scalable and feasible for a sulphur electrode. Figure 2A shows the top-view photo for the Al foil sequentially casted by sulphur layer, graphite and LTO with the average thickness of 23.6, and 8.9 and 23.9 μm respectively, as revealed by the scanning electron microscope (SEM) images in Figures 2B-2D. The corresponding energy-dispersive X-ray (EDX) mappings in Figures 2E-2G confirm that the sulphur, Super P® and binder molecules in the cathode are uniformly distributed, and they are fully covered by the graphite and LTO. Although the LTO is a typical anode in lithium ion battery, its embarrassing voltage at around 1.55 V is too high as an anode and also too low as an individual cathode. Uniquely herein, we show that the 1.55 V discharge voltage platform can be a perfect marriage with the voltage platform of 2.35 V and 2.1 V in lithium-sulphur battery, under which the LTO not only has the contribution to capacity and voltage, but it can also stabilize the cathode by blocking the dissolution/diffusion of polysulfide and act as a host for the insertion of lithium ions in its crystalline channels, thereby maximally avoiding the self-discharge of polysulfide on anode to form Li_2S. Further, the "zero-volume" expansion[40] and non-flammable properties of LTO capping layer are very attractive for enhancing the safety of battery.

Electrochemical Analysis

The stability of sulphur rich electrode and the effects of blocking layer sequence are further studied by electrochemical characterizations. In the open-circuit voltage (OCV) *vs.* time curves (Figure 3A), the initial OCV of the cell with the graphite/LTO and LTO/graphite is 2.83 V and 2.81 V respectively, much higher than 2.41 V for the cell without any blocking layer. The persevered high OCV confirms the efficiency of the composite layer for stabilizing the cathode and avoiding any self-discharge involved in the reactions between lithium and sulphur, which is rarely reported before. In cyclic voltammetry (CV) of the cell with LTO/graphite layer (Figure 3B), the clearly separated reduction peaks of 2.35V and 2.1 demonstrate the continued reduction process from S_8 to Li_2S_8 and Li_2S_6, and then to Li_2S_x ($1 \leq x \leq 6$) stepwise,[13] as manifested in the voltage *vs.* capacity profiles in Figure 1B. Meanwhile, the presence of forks in the oxidation peaks around 2.42 V, corresponding to the final oxidation of Li_2S_8 to S_8,[49] confirms the uniform distribution of trapped polysulfide (Li_2S_x, $1 \leq x \leq 8$) in specific areas with the help of dual blocking layer.

Note that the OCV decay of the cell with the graphite/LTO blocking layer from 2.83V to stabilized 2.44 V is faster than that of the cell with a LTO/graphite layer,

demonstrating that the lithium ion diffusion within the graphite/LTO layer is faster. The lithium ion diffusion constant between electrodes can be estimated using the *Randles-Sevcik* equation:

$$i_p = 2.69 \times 10^5 \, n^{\frac{3}{2}} A D^{\frac{1}{2}} C v^{\frac{1}{2}}$$

where i_p indicates the peak current, n is the number of electron in the reaction, A is the electrode area, υ is the scanning rate and C is the variation of lithium-ion concentration in the electrolyte.[3] The plot of normalized peak current (i_p) with the square root of the scan rate ($\upsilon^{1/2}$) is displayed in Figure 3C and the value of the diffusion constant is extracted as 1.15×10^{-7} cm^2 s^{-1} for the cell with graphite/LTO layer, which is indeed faster than 7.28×10^{-8} cm^2 s^{-1} of that with graphite/LTO layer. The order of magnitude of these values is comparable to recent result[50] and much higher than metal oxide cathode in lithium ion battery.[51] It indicate that the impact of adopting composite blocking layers to the lithium ion diffusion constant is limited particularly for the layer of graphite/LTO. This could be due to the rich boundaries of layers and crystalline channels of LTO which are sufficient enough for the transport of lithium ions. The Niquist plot (Figure 3D) for aged electrodes in electrochemical impedance spectroscopy (EIS) studies suggests that the direct contact of the graphite layer to sulphur helps to increase the electrical conductivity of electrodes, where the electrode-charge resistance for the graphite/LTO is 32.4 Ω, lower than 52.5 Ω for the LTO/graphite and 324.3 Ω of the pristine electrode. Furthermore, the highest slope of the graphite/LTO at high frequencies confirms its superior lithium ion diffusion than the LTO/graphite.

Visualization of S-dissolution and Operando Raman spectrum

The dissolution and diffusion of polysulphides with charge/discharge cycles can be visually observed using a home made glass tube battery, where a lithium foil, a separator, blocking layer, and a cathode can be assembled in the middle of the glass tube. A small chamber right next to the battery is designed to host electrolytes, which allows the confocal laser light to probe the signals of electrolytes simultaneously (see Figure 8 for details of the set-up). First, the dissolution of sulphur can be directly visualized by the colour change of the electrolyte from colourless to yellow with the cycling. Figures 4A, 4B and 4C demonstrate that the colour of the electrolyte for the cell without a blocking (Figure 4C) turns darkest at the 50th cycle, indicating the dissolution of sulphur species in electrolytes is pronounced. The cell with the graphite/LTO (Figure 4A) shows the lightest yellow colour among the three cells, corroborating that the graphite/LTO exhibits the best blocking performance for sulphur species.

We analyse the operando Raman spectra for the initial 50 cycles of three different cells. One obvious observation is that the baseline (background) of the spectra shifts up with the progress of charge/discharge cycle (Figure 4D), which is attributed to the scattering of the laser light caused by the dissolution of sulphur species in electrolytes (Figures 9A-B). We plot the arbitrary intensity of the baseline at 2500 cm^{-1} as a function of cycle number for three cells. Figure 4E shows that the relative intensity of the baseline for the cell without a blocking layer is the highest at the 50^{th} cycle, consistent with the visual observation in Figures 4A-4C. Note that the baseline intensity increase for the cell without a blocking layer does not show significant difference with other two cells in initial cycles but it deviates quickly with cycling. This suggests that the dissolution of polysulphides is an accumulation process and then gives rise to the highest baseline intensity (*vs.* darkest colour of the electrolyte) (Figure 4E). In Raman spectra, one can identify the symmetric stretching mode of typical $S_3^{\cdot-}$ species at around 534 cm^{-1} (Figure 4G-4I),[52] where the results again suggest that the LTO/graphite layer is the most efficient blocking structure because of its weakest Raman signal at 534 cm^{-1}.

Reaction Process

The cycled sulphur electrodes are disassembled from the coin cell and characterized by the energy-dispersive X-ray (EDX) to reveal the evolution of electrode with cycling. Based on the experimental observations, we proposed a model to interpret the high capacity from graphite/LTO capped sulphur electrode. When the sulphur-rich electrode is assembled to the battery without capping layers, the reaction $Li^+ + S_8 + e^- \rightarrow Li_2S_x$ (x = 1-8) shall happen and certain amount of sulphur may be reacted as confirmed by the emergence of $S_3^{\cdot-}$ in Raman. However, the EIS result shows that the electrical resistance of the pristine sulphur cathode is high and thus the reaction between sulphur and lithium ions is limited. In the discharge process, the reaction lithium ion and sulphur is still prohibited because of the low electrical transport, thereby giving rise to a very low capacity and large voltage polarization (Fig. 6A). Only the bottom sulphur particles close to the aluminium foil (current collector) have a high chance to react since they are closer to the current collector. The reaction and dissolution of sulphur particles close to the Al foil in initial cycles lead to the gradual precipitation of PVDF binder molecules and Super P® carbon on Al surface, as confirmed by the SEM/EDXA results in which the sulphur is gradually removed with cycling (Figure 5A-5C). With the extended cycling, the sulphur electrode can be easily peeled from the Al current collector due to the interfacial

precipitation of PVDF (inset of Figure 5C). Figure 5D shows the schematics for the proposed reaction mechanism.

When the sulphur rich cathode is covered by the graphite layer, the graphite particles fill in the vacant areas between sulphur particles. And then the electrode was further covered by the layer of LTO (Figure 5E). In this way, the graphite layer contacts well with the aluminium foil, sulphur cathode and LTO layer together even for cycling (Figure 5F, 5G), thereby providing a better pathway for charge movement (Figure 5H). Thus, the sulphur utilization can achieve 100% because the protection of dual layer which avoids the sulphur pre-dissolution and faster charge movement. The higher sulphur utilization of battery using graphite/LTO layer than that of pristine electrode was further confirmed by the current value under CV curves (Figure 3B). For example, the current of battery using graphite/layer can achieve 7.5 mA at 0.01 mV s^{-1} while the battery with pristine electrode only shows the value less than 0.1 mA (inset of Figure 3B). Benefiting from the covering of dual layer, the dissolution and diffusion of polysulfide was largely suppressed, particularly the LTO can host the lithium ions at the voltage of 1.55 V under which it can effectively avoid the formation of Li_2S on anode. During the cycling, the cathode remains integrated as revealed in inset of Figure 5G, and the reaction process was presented in Figure 5H. Together with the robust layer protection ability, fast lithium diffusion constant and low electric resistance, they are responsible for the high utilization of sulphur in the structure with graphite/LTO.

Conclusion

A new hybrid lithium-sulphur battery with exceptional capacity over 1866 mAh g^{-1} and multi-voltage platforms from 2.35 V, 2.1 V to 1.55 V were presented. The energy density over 3863 Wh kg^{-1} is at least ten times higher than lithium ion battery and also superior than the theoretical 2600 Wh kg^{-1} of lithium-sulphur battery. An efficient dual blocking layer of graphite/$Li_4Ti_5O_{12}$ was presented for the first time to get a 100% utilization of sulphur cathode. The battery using graphite/LTO blocking layer has the robust capacity around 1226 mAh g^{-1} at the high rate of 1C with endurable cycle life over 100 cycles. The hybrid lithium battery with the concept of composite layers may stimulate the research to marry various materials with lithium storage capacity for future energy storage and conversion devices.

References for Example 1

1 P. G. Bruce, S. A. Freunberger, L. J. Hardwick and J. M. Tarascon, *Nat. Mater.*, 2012. 11, 19-29.

2 B. Scrosati, J. Hassoun and Y. K. Sun, *Energy Environ. Sci.*, 2011. 4, 3287-3295.

3 H. G. Jung, J. Hassoun, J. B. Park, Y. K. Sun and B. Scrosati, *Nat. Chem.*, 2012. 4, 579-585.

4 Z. Q. Peng, S. A. Freunberger, Y. H. Chen and P. G. Bruce, *Science*, 2012. 337, 563-566.

5 Q. C. Liu, J. J. Xu, D. Xu and X. B. Zhang, *Nat. Commun.*, 2015. 6, DOI: 10.1038/ncomms8892.

6 J. Lu, L. Li, J. B. Park, Y. K. Sun, F. Wu and K. Amine, *Chem. Rev.*, 2014. 114, 5611-5640.

7 R. Demir-Cakan, M. Morcrette, Gangulibabu, A. Gueguen, R. Dedryvere and J. M. Tarascon, *Energy Environ. Sci.*, 2013. 6, 176-182.

8 A. Manthiram, Y. Z. Fu, S. H. Chung, C. X. Zu and Y. S. Su, *Chem. Rev.*, 2014. 114, 11751-11787.

9 S. Evers and L. F. Nazar, *Acc. Chem. Res.*, 2013. 46, 1135-1143.

10 Urbonaite, T. Poux and P. Novák, *Adv. Energy Mater.*, 2015. 5, DOI: 10.1002/aenm.201500118.

11 S. K. Lee, S. M. Oh, E. Park, B. Scrosati, J. Hassoun, M. S. Park, Y. J. Kim, H. Kim, I. Belharouak and Y. K. Sun, *Nano Lett.*, 2015. 15, 2863-2868.

12 T. Ohzuku and Y. Makimura, *Chem. Lett.,* 2001, 642-643.

13 Y. V. Mikhaylik and J. R. Akridge, *J. Electrochem. Soc.*, 2004. 151, A1969-A1976.

14 L. Wang, Y. G. Wang and Y. Y. Xia, *Energy Environ. Sci.*, 2015. 8, 1551-1558.

15 M. Agostini, S. Z. Xiong, A. Matic and J. Hassoun, *Chem. Mater.*, 2015. 27, 4604-4611.

16 X. L. Ji, K. T. Lee and L. F. Nazar, *Nat. Mater.*, 2009. 8, 500-506.

17 G. He, X. L. Ji and L. Nazar, *Energy Environ. Sci.*, 2011. 4, 2878-2883.

18 N. Jayaprakash, J. Shen, S. S. Moganty, A. Corona and L. A. Archer, *Angew. Chem. Int. Ed.*, 2011. 50, 5904-5908.

19 J. Kim, D. J. Lee, H. G. Jung, Y. K. Sun, J. Hassoun and B. Scrosati, *Adv. Funct. Mater.*, 2013. 23, 1076-1080.

20 J. C. Guo, Y. H. Xu and C. S. Wang, *Nano Lett.*, 2011. 11, 4288-4294.

21 G. M. Zhou, D. W. Wang, F. Li, P. X. Hou, L. C. Yin, C. Liu, G. Q. Lu, I. R. Gentle and H. M. Cheng, *Energy Environ. Sci.*, 2012. 5, 8901-8906.

22 22. L. W. Ji, M. M. Rao, H. M. Zheng, L. Zhang, Y. C. Li, W. H. Duan, J. H. Guo, E. J. Cairns and Y. G. Zhang, *J. Am. Chem. Soc.*, 2011. 133, 18522-18525.

23 Z. W. Seh, W. Y. Li, J. J. Cha, G. Y. Zheng, Y. Yang, M. T. McDowell, P. C. Hsu and Y. Cui, *Nat. Commun.*, 2013. 4, 1331.

24 H. L. Wang, Y. Yang, Y. Y. Liang, J. T. Robinson, Y. G. Li, A. Jackson, Y. Cui and H. J. Dai, *Nano Lett.*, 2011. 11, 2644-2647.

25 W. D. Zhou, Y. C. Yu, H. Chen, F. J. DiSalvo and H. D. Abruna, *J. Am. Chem. Soc.*, 2013. 135, 16736-16743.

26 J. L. Wang, Z. D. Yao, C. W. Monroe, J. Yang and Y. Nuli, *Adv. Funct. Mater.*, 2013. 23, 1194-1201.

27 J. Hassoun and B. Scrosati, *Angew. Chem. Int. Ed.*, 2010. 49, 2371-2374.

28 M. Agostini and J. Hassoun, *Sci. Rep.*, 2015. 5, 7591.

29 Z. Lin, Z. C. Liu, W. J. Fu, N. J. Dudney and C. D. Liang, *Angew. Chem. Int. Ed.*, 2013. 52, 7460-7463.

30 S. S. Zhang, *Electrochimica Acta*, 2012. 70, 344-348.

31 X. L. Ji, S. Evers, R. Black and L. F. Nazar, *Nat. Commun.*, 2011. 2, 325.

32 Y. Z. Fu, Y. S. Su and A. Manthiram, *Angew. Chem. Int. Ed.*, 2013. 52, 6930-6935.

33 M. Agostini, B. Scrosati and J. Hassoun, *Adv. Energy Mater.*, 2015. 5. DOI: 10.1002/aenm.201500481.

34 Y. Z. Fu, Y. S. Su and A. Manthiram, *Adv. Energy Mater.*, 2014. 4, 1300655.

35 Y. S. Su and A. Manthiram, *Nat. Commun.*, 2012. 3, 1166.

36 C. Huang, J. Xiao, Y. Y. Shao, J. M. Zheng, W. D. Bennett, D. P. Lu, L. V. Saraf, M. Engelhard, L. W. Ji, J. G. Zhang, X. L. Li, G. L. Graff and J. Liu, *Nat. Commun.*, 2014. 5, 3343.

37 S. H. Chung and A. Manthiram, *Adv. Funct. Mater.*, 2014. 24, 5299-5306.

38 J. Q. Huang, Q. Zhang, H. J. Peng, X. Y. Liu, W. Z. Qian and F. Wei, *Energy Environ. Sci.*, 2014. 7, 347-353.

39 G. Q. Ma, Z. Y. Wen, M. F. Wu, C. Shen, Q. S. Wang, J. Jin and X. W. Wu, *Chem. Commun.*, 2014. 50, 14209-14212.

40 K. Zaghib, M. Simoneau, M. Armand and M. Gauthier, *J. Power Sources*, 1999. 81, 300-305.

41 H. G. Jung, M. W. Jang, J. Hassoun, Y. K. Sun and B. Scrosati, *Nat. Commun.*, 2011. 2, 516.

42 H. W. Chen, C. H. Wang, W. L. Dong, W. Lu, Z. L. Du and L. W. Chen, *Nano Lett.*, 2015. 15, 798-802.

43 S. Xin, L. Gu, N. H. Zhao, Y. X. Yin, L. J. Zhou, Y. G. Guo and L. J. Wan, *J. Am. Chem. Soc.*, 2012. 134, 18510-18513.

44 L. W. Ji, M. M. Rao, S. Aloni, L. Wang, E. J. Cairns and Y. G. Zhang, *Energy & Environmental Science*, 2011. 4, 5053-5059.

45 Y. S. Su, Y. Z. Fu, T. Cochell and A. Manthiram, *Nat. Commun.*, 2013. 4, 2985.

46 G. M. Zhou, E. Paek, G. S. Hwang and A. Manthiram, *Nat. Commun.*, 2015. 6, 7760.

47 J.-Y. Hwang, H. M. Kim, S.-K. Lee, J.-H. Lee, A. Abouimrane, M. A. Khaleel, I. Belharouak, A. Manthiram and Y.-K. Sun, *Adv. Energy Mater.*, 2015, DOI: 10.1002/aenm.201501480.

48 J. Q. Huang, X. F. Liu, Q. Zhang, C. M. Chen, M. Q. Zhao, S. M. Zhang, W. C. Zhu, W. Z. Qian and F. Wei, *Nano Energy*, 2013. 2, 314-321.

49 H.-D. Shin, M. Agostini, I. Belharouak, J. Hassoun and Y.-K. Sun, *Carbon*, 2016. 96, 125-130.

50 J. Q. Huang, T. Z. Zhuang, Q. Zhang, H. J. Peng, C. M. Chen and F. Wei, *ACS Nano*, 2015. 9, 3002-3011.

51 M. Park, X. C. Zhang, M. D. Chung, G. B. Less and A. M. Sastry, *J. Power Sources*, 2010. 195, 7904-7929.

52 H. L. Wu, L. A. Huff and A. A. Gewirth, *ACS Appl. Mater. Interfaces,* 2015. 7, 1709-1719.

Example 2

Table 1 Theoretical capacity of lithium-sulfur battery in step-sized electrochemical reactions.

Main step-sized electrochemical reactions	Theoretical capacity/ mAh g^{-1}†
$S_8 + 2Li^+ + 2e^- \rightarrow Li_2S_8$	209.38
$Li_2S_8 + 2/3Li^+ + 2/3e^- \rightarrow 4/3Li_2S_6$ ($2S_3^{\bullet-}$)	69.79
$Li_2S_6 + Li^+ + e^- \rightarrow 3/2Li_2S_4$	139.59
$Li_2S_4 + 2/3Li^+ + 2/3e^- \rightarrow 4/3Li_2S_3$	139.59
$Li_2S_3 + Li^+ + e^- \rightarrow 3/2Li_2S_2$	279.18
$Li_2S_2 + 2Li^+ + 2e^- \rightarrow 2Li_2S$	837.54

†Theoretical capacity was calculated by the equation of C = NA*q*n/3.6/M_s, in which NA, q, n and M_s are the Avogadro constant (i.e., 6.02214 × 10^{23} mol^{-1}), elementary charge (i.e., 1.602176 × 10^{-19} C, 1 mAh = 3.6 C), number of transferred electron and molar mass of sulfur participated in the reaction respectively.

Table 2 Capacity ratio of Q_1/Q_{slop} and $(Q_1+ Q_{slope})/Q_2$ in the 1st cycle compared with previous results.

Kind of Electrode†	Total Capacity	Q_1	Q_{slope}	Q_2	Q_{solpe}/Q_1 *vs.* $(Q_1+Q_{slope})/Q_2$††	Reference
Super P®-S@graphite@LTO	1675	321	218	1136	0.679 *vs.* 0.474	This work
CMK-3/S	1000	133	87	780	0.654 *vs.* 0.282	[1]
S-TiO_2 yolk-shell (0.2C)	1010	225	125	660	0.556 *vs.* 0.530	[2]
Porous carbon spheres/S	1190	190	120	880	0.6315 *vs.* 0.352	[3]
Graphene-S	1500	300	200	1000	0.667 *vs.* 0.500	[4]
Carbon spheres/S (0.25C)	800	<20	<10	~770	0.500 *vs.* 0.039	[5]
Sulfur-rich polymer (0.2C)	1050	200	100	750	0.500 *vs.* 0.400	[6]
S@GDL (0.12C)	1300	200	130	970	0.650 *vs.* 0.340	[7]
Carbon nanotube/$NiFe_2O_4$−S	1350	250	150	950	0.600 *vs.* 0.421	[8]
N-doped hollow carbon/S	1140	200	130	810	0.520 *vs.* 0.407	[9]
Polyacrylonitrile/S (0.2C)	1300	200	110	990	0.550 *vs.* 0.313	[10]
S/MnO_2 (0.05C)	1300	250	150	900	0.600 *vs.* 0.444	[11]
S/hollow mesoporous titania@Carbon nanotubes	1560	300	150	1110	0.500 *vs.* 0.405	[12]
Stacked graphene-S	1200	250	150	800	0.600 *vs.* 0.500	[13]
S/Ti_2C (Mxene) (0.05C)	1420	265	165	1000	0.6226 *vs.* 0.420	[14]

†If without noting the current density, the electrode was performed at the rate of 0.1°C.

††The ratio of Q_{slope}/Q_1 and $(Q_1+ Q_{slope})/Q_2$ are more accurate for comparing the results because it can avoid the error resulted from the mass of active materials (i.e., sulfur) in the electrode. The longer discharge curve of Q_{slope} comparing to Q_1 with the highest ratio value of 0.679 demonstrate that a lot of soluble sulfur species are well trapped in the blocking layer and then could be reacted to contribute a high capacity. And also, a high ratio of $(Q_1+ Q_{slope})/Q_2$ demonstrate that a good protection of sulfur species avoiding from their dissolution/migration towards lithium anode side.

References for Example 2

1. X. L. Ji, K. T. Lee and L. F. Nazar, *Nat. Mater.*, 2009. **8**, 500-506.

2. Z. W. Seh, W. Y. Li, J. J. Cha, G. Y. Zheng, Y. Yang, M. T. McDowell, P. C. Hsu and Y. Cui, *Nat. Commun.*, 2013. **4**, 1331.

3. J. Liu, T. Y. Yang, D. W. Wang, G. Q. M. Lu, D. Y. Zhao and S. Z. Qiao, *Nat. Commun.*, 2013. **4**, 2798.

4. T. Q. Lin, Y. F. Tang, Y. M. Wang, H. Bi, Z. Q. Liu, F. Q. Huang, X. M. Xie and M. H. Jiang, *Energy Environ. Sci.*, 2013. **6**, 1283-1290.

5. B. Zhang, X. Qin, G. R. Li and X. P. Gao, *Energy Environ. Sci.*, 2010. **3**, 1531-1537.

6. H. Kim, J. Lee, H. Ahn, O. Kim and M. J. Park, *Nat. Commun.*, 2015. **6**, 7278.

7. S. K. Lee, S. M. Oh, E. Park, B. Scrosati, J. Hassoun, M. S. Park, Y. J. Kim, H. Kim, I. Belharouak and Y. K. Sun, *Nano Lett.*, 2015. **15**, 2863-2868.

8. Q. Fan, W. Liu, Z. Weng, Y. M. Sun and H. L. Wang, *J. Am. Chem. Soc.*, 2015. **137**, 12946-12953.

9. W. Zhou, X. Xiao, M. Cai and L. Yang, *Nano Lett.*, 2014. **14**, 5250-6.

10. S. Y. Wei, L. Ma, K. E. Hendrickson, Z. Y. Tu and L. A. Archer, *J. Am. Chem. Soc.*, 2015. **137**, 12143-12152.

11. X. Liang, C. Hart, Q. Pang, A. Garsuch, T. Weiss and L. F. Nazar, *Nat. Commun.*, 2015. **6**.

12. J.-Y. Hwang, H. M. Kim, S.-K. Lee, J.-H. Lee, A. Abouimrane, M. A. Khaleel, I. Belharouak, A. Manthiram and Y.-K. Sun, *Adv. Energy Mater.*, 2015, DOI: 10.1002/aenm.201500481.

13. M. Q. Zhao, Q. Zhang, J. Q. Huang, G. L. Tian, J. Q. Nie, H. J. Peng and F. Wei, *Nat. Commun.*, 2014. **5**, 3410.

14. X. Liang, A. Garsuch and L. F. Nazar, *Angew. Chem. Int. Ed.*, 2015. **54**, 3907-11.

It should be noted that ratios, concentrations, amounts, and other numerical data may be expressed herein in a range format. It is to be understood that such a range format is used for convenience and brevity, and thus, should be interpreted in a flexible manner to include not only the numerical values explicitly recited as the limits of the range, but also to include all the individual numerical values or sub-ranges encompassed within that range as if each numerical value and sub-range is explicitly recited. To illustrate, a concentration range of "about 0.1% to about 5%" should be interpreted to include not only the explicitly recited concentration of about 0.1 wt% to about 5 wt%, but also include individual concentrations

(*e.g.*, 1%, 2%, 3%, and 4%) and the sub-ranges (*e.g.*, 0.5%, 1.1%, 2.2%, 3.3%, and 4.4%) within the indicated range. In an embodiment, the term "about" can include traditional rounding according to how the numerical value determined. In addition, the phrase "about 'x' to 'y'" includes "about 'x' to about 'y'".

Many variations and modifications may be made to the above-described embodiments. All such modifications and variations are intended to be included herein within the scope of this disclosure and protected by the following claims.

CLAIMS

At least the following is claimed:

1. A battery, comprising:
an anode; and
a cathode, wherein a dual blocking layer is disposed on the cathode, wherein the dual blocking layer is a graphite/$Li_4Ti_5O_{12}$ dual layer, wherein the dual layer is between the anode and the cathode.

2. The battery of claim 1, wherein the cathode is a sulfur cathode and the battery is a lithium-sulfur battery.

3. The battery of claim 2, wherein the graphite portion of the dual layer is adjacent the sulfur cathode.

4. The battery of claim 1, wherein the $Li_4Ti_5O_{12}$ is spinel $Li_4Ti_5O_{12}$.

5. The battery of claim 2, wherein the battery has a capacity over about 1866 mAh/g.

6. The battery of claim 2, wherein the battery has an energy density over about 3860 Wh/kg.

7. The battery of claim 2, wherein the dual blocking layer has a capacity of about 1220 mAh/g at about 1 C for a life cycle of over about 100 cycles.

8. The battery of claim 2, wherein the battery has a sulfur utilization rate more than about 90%.

9. A battery, comprising:
an anode; and
a cathode, wherein a dual blocking layer is disposed on the cathode, wherein the dual blocking layer is a conductive material and a lithium storage medium, wherein the dual layer is between the anode and the cathode.

10. The battery of claim 9, wherein the conductive material is selected from the group consisting of: a carbon based material, a conductive polymer, and a combination thereof.

11. The battery of claim 10, wherein the carbon based material is selected from the group consisting of: graphite, conductive carbon black, active carbon, activated carbon, acetylene black, carbon nanotubes, graphene, graphene oxide, and combinations thereof.

12. The battery of claim 10, wherein the conductive polymer is selected from the group consisting of: polyaniline, polypyrrole, polythiophenes, PEDOT:PSS, chitosan, and a combination thereof.

13. The battery of claim 9, wherein the lithium storage medium is selected from the group consisting of: $Li_4Ti_5O_{12}$, TiO_2, MoO_2, Fe_2O_3, Co_3O_4, MoS_2, and a combination thereof.

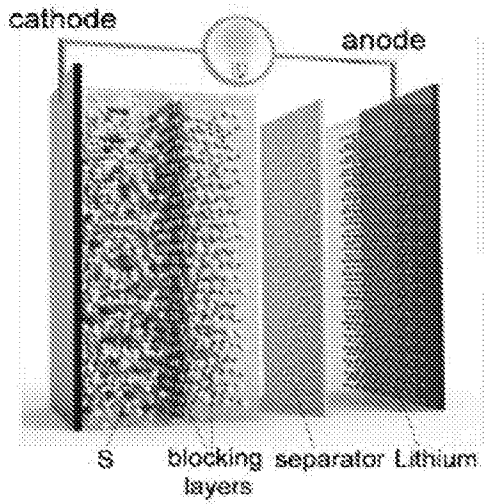

Fig. 1A

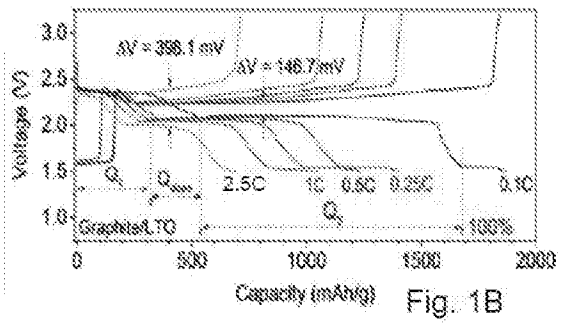

Fig. 1B

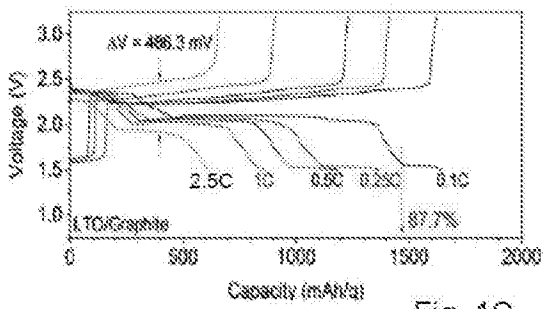

Fig. 1C

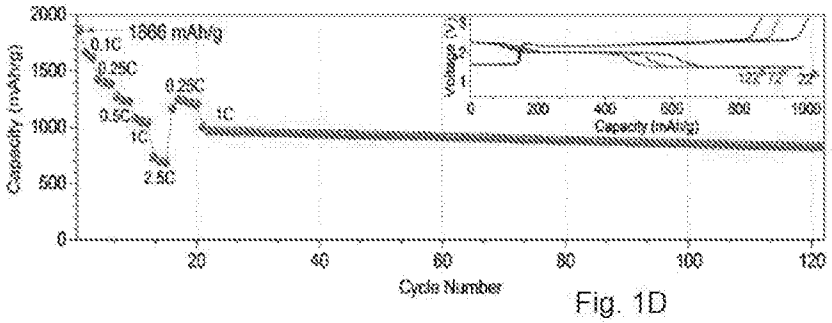

Fig. 1D

Fig. 2A

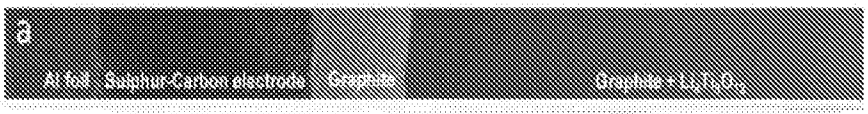

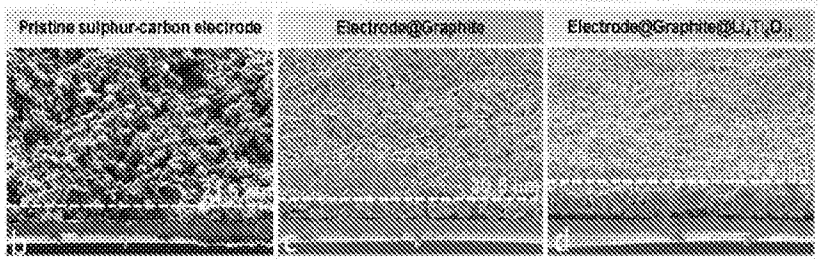

Fig. 2B Fig. 2C Fig. 2D

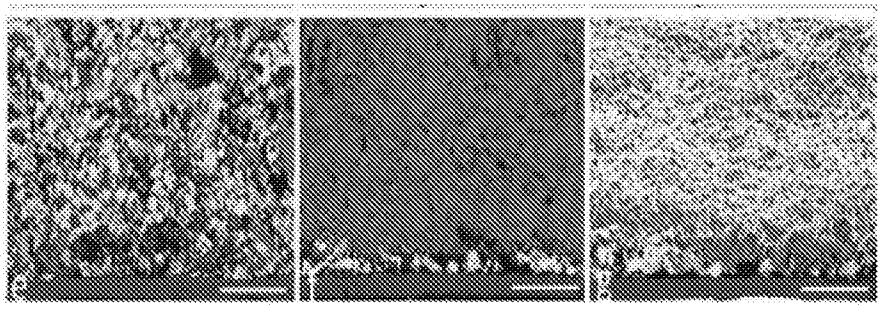

Fig. 2E Fig. 2F Fig. 2G

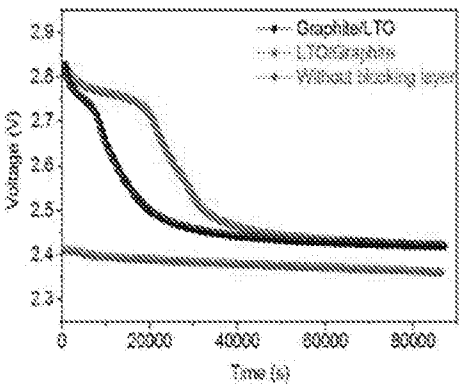

Fig. 3A

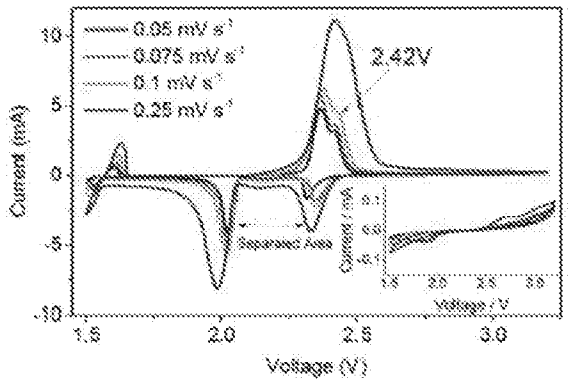

Fig. 3B

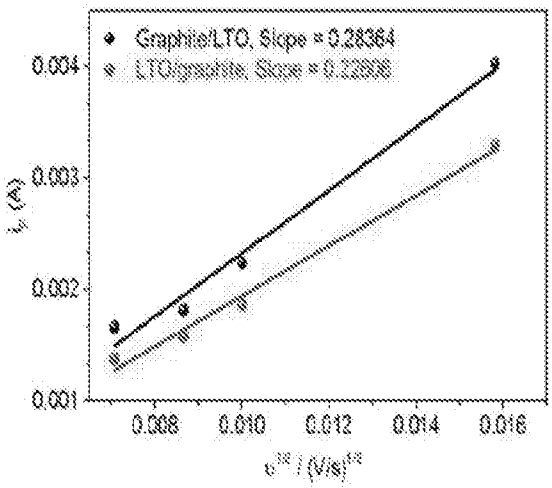
Graphite/LTO, Slope = 0.28364
LTO/graphite, Slope = 0.22808
0.004
0.003
0.002
0.001
0.008
0.010
0.012
0.014
0.016

Fig. 3C

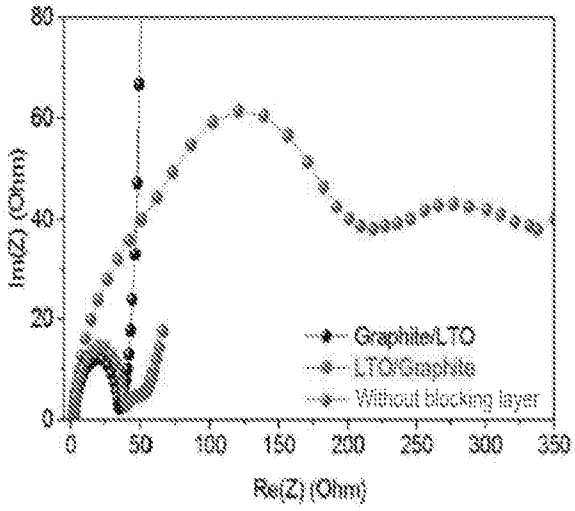
80
60
40
20
0
0
50
100
150
200
250
300
350
Im(Z) (Ohm)
Re(Z) (Ohm)
Graphite/LTO
LTO/Graphite
Without blocking layer

Fig. 3D

Fig. 4A Fig. 4B Fig. 4C

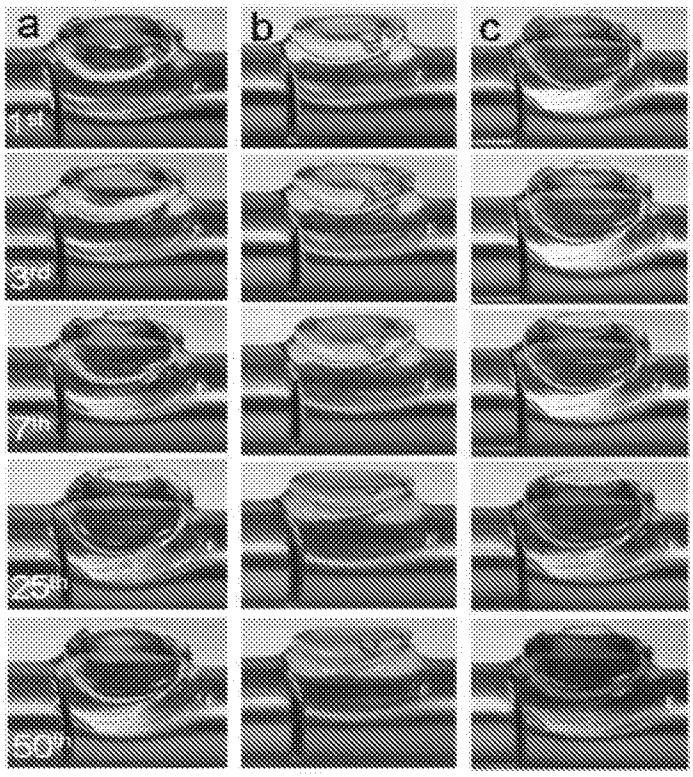

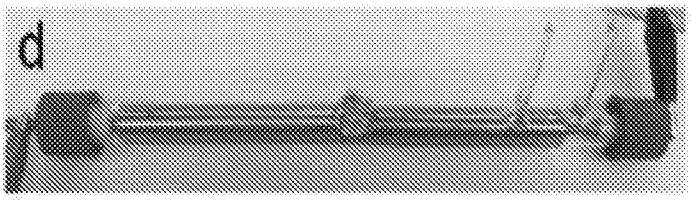

Fig. 4D

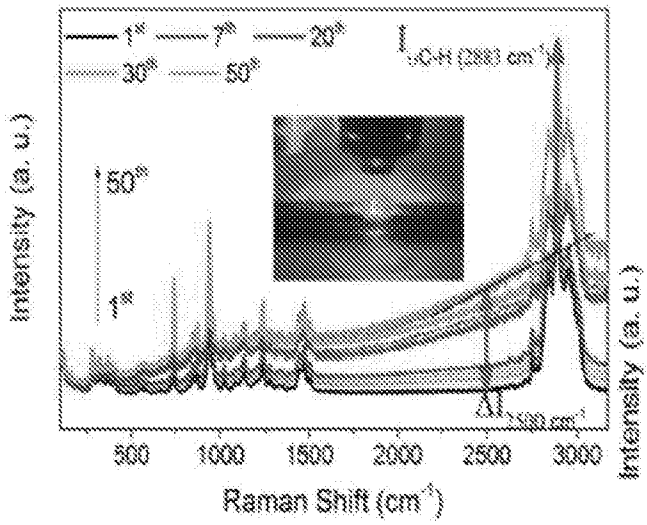

Fig. 4E

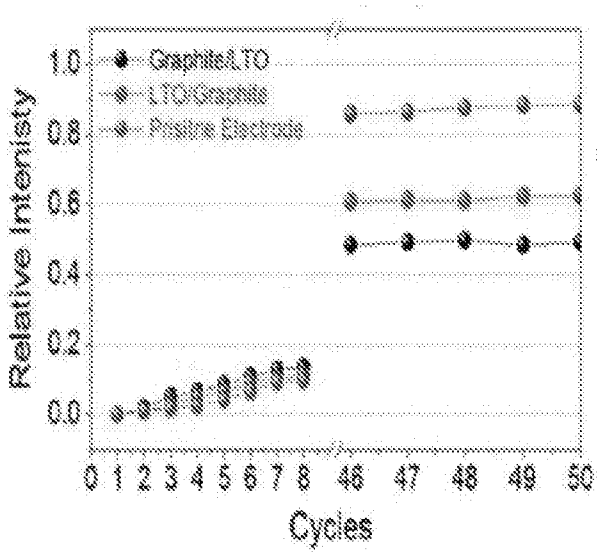

Fig. 4F

Fig. 4G

Fig. 4H

Fig. 4I

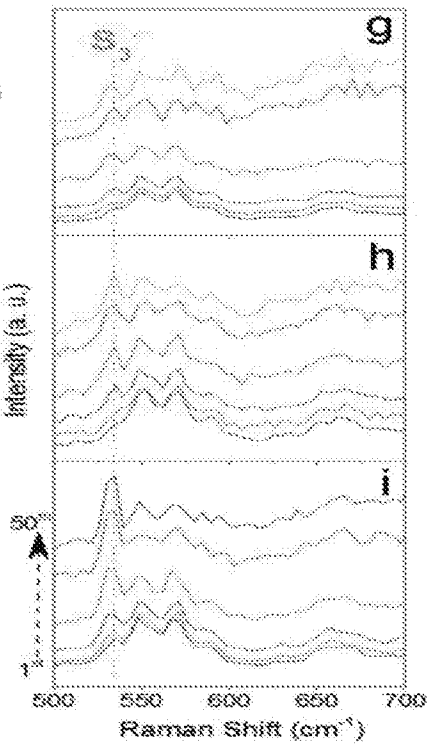

Fig. 5A

Fig. 5B

Fig. 5C

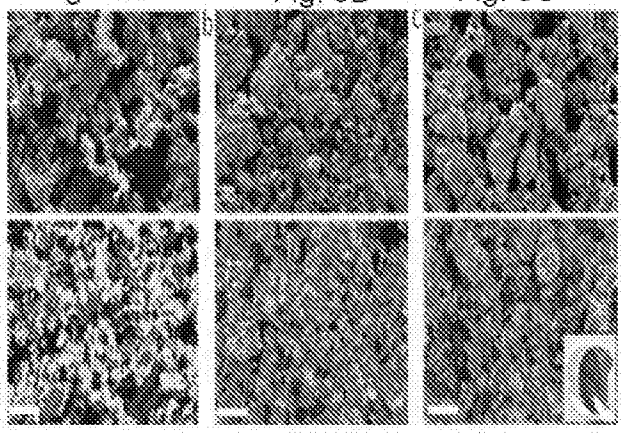

Fig. 5D

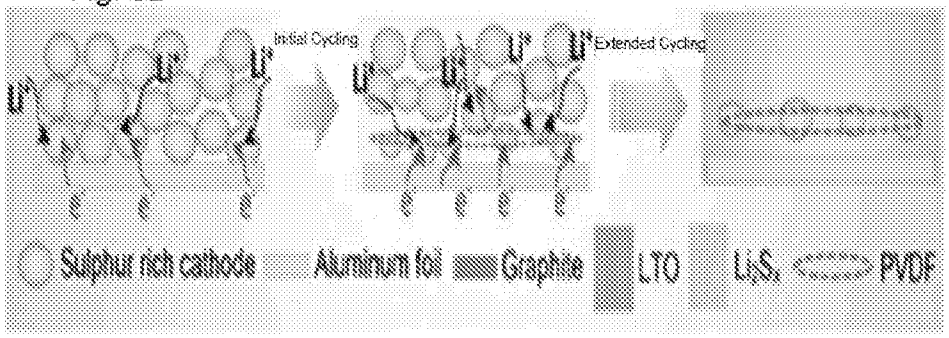

Fig. 5E

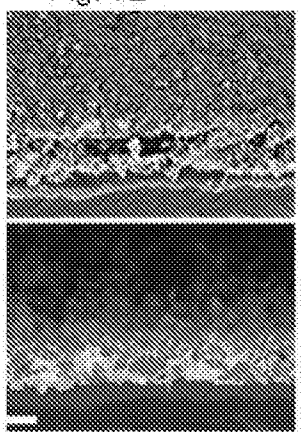

Fig. 5F

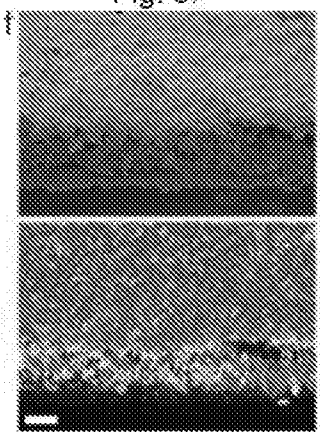

Fig. 5G

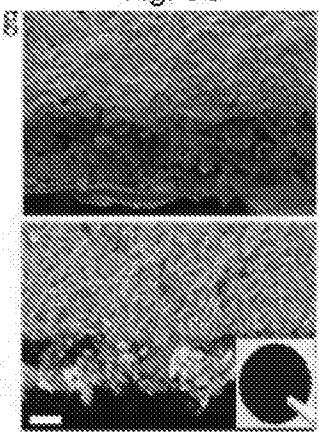

Fig. 5H

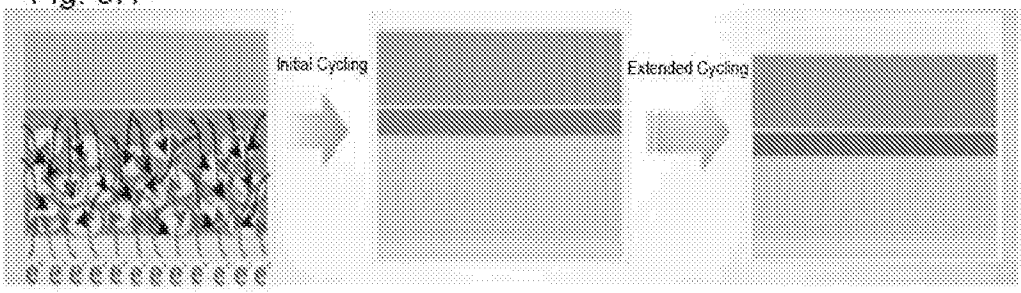
Initial Cycling
Extended Cycling

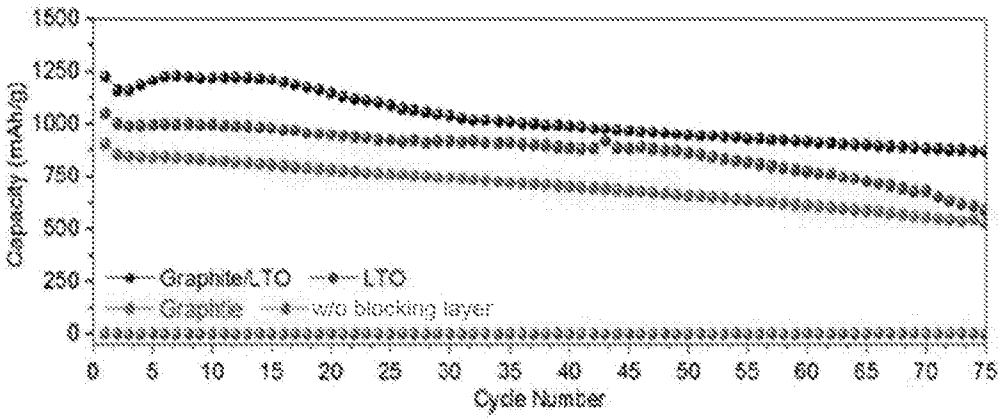
1500
1250
1000
750
500
250
0
Capacity (mAh/g)
Graphite/LTO
LTO
Graphite
w/o blocking layer
0
5
10
15
20
25
30
35
40
45
50
55
60
65
70
75
Cycle Number

Fig. 6A

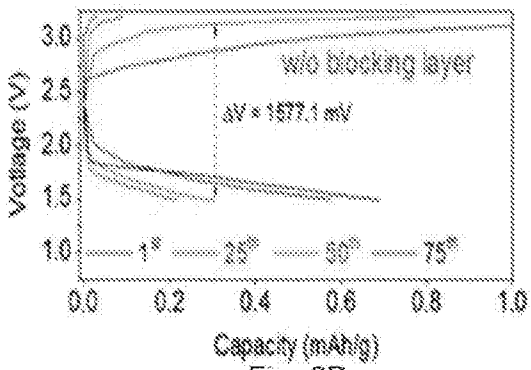

Fig. 6B

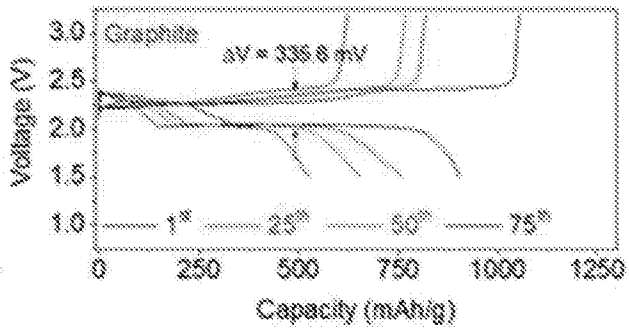

Fig. 6C

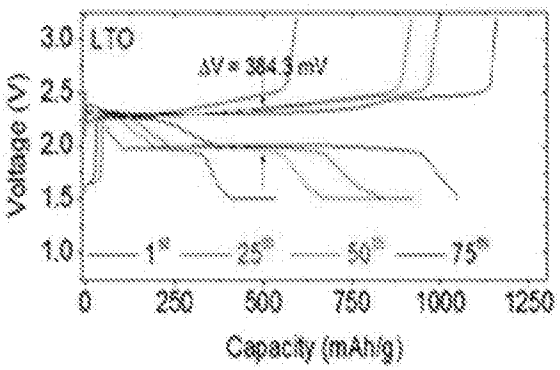

Fig. 6D

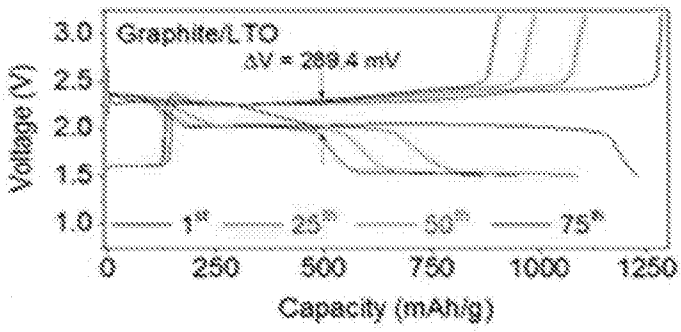

Fig. 6E

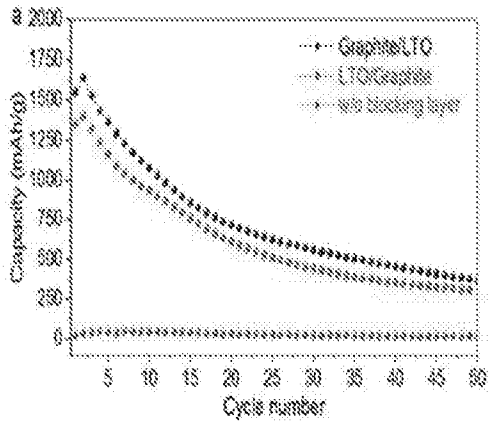

Fig. 7A

Fig. 7B

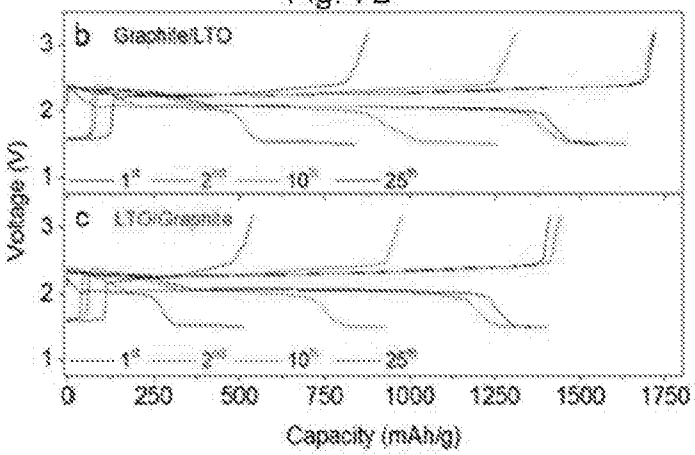

Fig. 7C

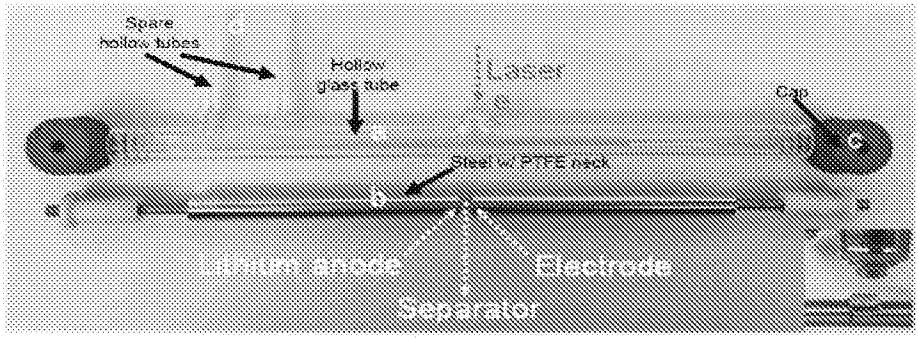

Fig. 8

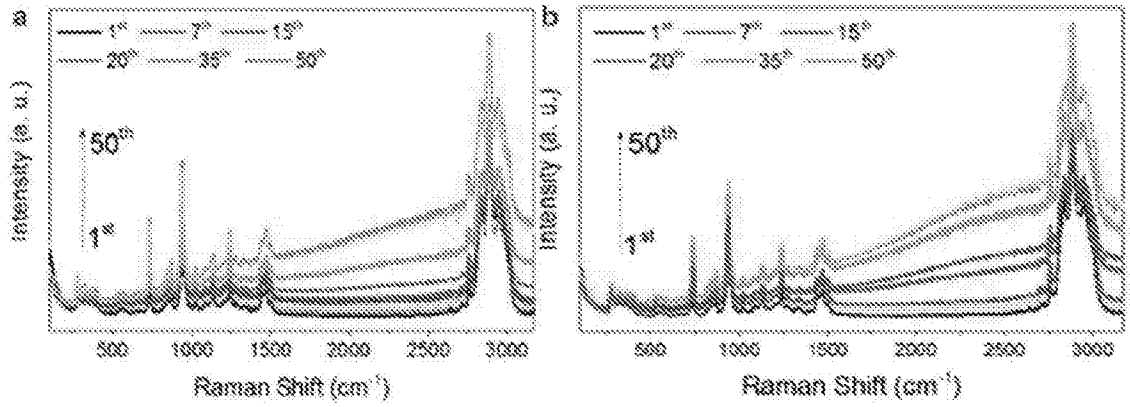

Fig. 9A

Fig. 9B

INTERNATIONAL SEARCH REPORT

International application No
PCT/IB2016/057574

A. CLASSIFICATION OF SUBJECT MATTER
INV. H01M4/38 H01M4/485 H01M4/62
ADD.

According to International Patent Classification (IPC) or to both national classification and IPC

B. FIELDS SEARCHED

Minimum documentation searched (classification system followed by classification symbols)
H01M

Documentation searched other than minimum documentation to the extent that such documents are included in the fields searched

Electronic data base consulted during the international search (name of data base and, where practicable, search terms used)
EPO-Internal, WPI Data

C. DOCUMENTS CONSIDERED TO BE RELEVANT

Category*	Citation of document, with indication, where appropriate, of the relevant passages	Relevant to claim No.
A	US 2015/084604 A1 (THILLAIYAN RAMANATHAN [US] ET AL) 26 March 2015 (2015-03-26) paragraph [0072]	1-13
A	US 2013/309572 A1 (ZHANG SHENGSHUI [US] ET AL) 21 November 2013 (2013-11-21) claim 1	1-13
A	US 2015/221937 A1 (KIM YONG-TAE [KR] ET AL) 6 August 2015 (2015-08-06) paragraphs [0078] - [0079]	9-13

-/--

[X] Further documents are listed in the continuation of Box C.

[X] See patent family annex.

* Special categories of cited documents :

"A" document defining the general state of the art which is not considered to be of particular relevance

"E" earlier application or patent but published on or after the international filing date

"L" document which may throw doubts on priority claim(s) or which is cited to establish the publication date of another citation or other special reason (as specified)

"O" document referring to an oral disclosure, use, exhibition or other means

"P" document published prior to the international filing date but later than the priority date claimed

"T" later document published after the international filing date or priority date and not in conflict with the application but cited to understand the principle or theory underlying the invention

"X" document of particular relevance; the claimed invention cannot be considered novel or cannot be considered to involve an inventive step when the document is taken alone

"Y" document of particular relevance; the claimed invention cannot be considered to involve an inventive step when the document is combined with one or more other such documents, such combination being obvious to a person skilled in the art

"&" document member of the same patent family

Date of the actual completion of the international search	Date of mailing of the international search report
1 February 2017	09/02/2017

Name and mailing address of the ISA/	Authorized officer
European Patent Office, P.B. 5818 Patentlaan 2 NL - 2280 HV Rijswijk Tel. (+31-70) 340-2040, Fax: (+31-70) 340-3016	Letilly, Marika

INTERNATIONAL SEARCH REPORT

International application No
PCT/IB2016/057574

C(Continuation). DOCUMENTS CONSIDERED TO BE RELEVANT

Category*	Citation of document, with indication, where appropriate, of the relevant passages	Relevant to claim No.
A	VALÉRY WEBER ET AL: "Computational Study of Lithium Titanate as a Possible Cathode Material for Solid-State Lithium-Sulfur Batteries", JOURNAL OF PHYSICAL CHEMISTRY C, vol. 119, no. 18, 7 May 2015 (2015-05-07), pages 9681-9691, XP055252604, US ISSN: 1932-7447, DOI: 10.1021/jp5105455 figure 1	1-13
A	US 2013/337293 A1 (EISELE ULRICH [DE] ET AL) 19 December 2013 (2013-12-19) paragraph [0038]; figure 1	1-13
A	US 2015/056507 A1 (DADHEECH GAYATRI VYAS [US] ET AL) 26 February 2015 (2015-02-26) paragraphs [0031] - [0032]	9-13
A	JP 2012 014892 A (SUMITOMO ELECTRIC INDUSTRIES) 19 January 2012 (2012-01-19) paragraph [0046]	1

INTERNATIONAL SEARCH REPORT

Information on patent family members

International application No
PCT/IB2016/057574

Patent document cited in search report	Publication date	Patent family member(s)	Publication date
US 2015084604 A1	26-03-2015	AU 2014233600 A1	09-04-2015
		CA 2864498 A1	26-03-2015
		GB 2523613 A	02-09-2015
		US 2015084604 A1	26-03-2015
US 2013309572 A1	21-11-2013	NONE	
US 2015221937 A1	06-08-2015	KR 101365679 B1	20-02-2014
		US 2015221937 A1	06-08-2015
		WO 2014027841 A1	20-02-2014
US 2013337293 A1	19-12-2013	CN 103270641 A	28-08-2013
		DE 102010064302 A1	05-07-2012
		EP 2659541 A1	06-11-2013
		JP 5762562 B2	12-08-2015
		JP 2014501436 A	20-01-2014
		KR 20130143621 A	31-12-2013
		US 2013337293 A1	19-12-2013
		WO 2012089383 A1	05-07-2012
US 2015056507 A1	26-02-2015	CN 105765771 A	13-07-2016
		DE 112014003358 T5	07-04-2016
		US 2015056507 A1	26-02-2015
		WO 2015026951 A1	26-02-2015
JP 2012014892 A	19-01-2012	NONE	